Quantifying B-Mode Images of In Vivo Rat Mammary Tumors by the Frequency Dependence of Backscatter

Karen A. Topp, PhD, James F. Zachary, DVM, PhD, William D. O'Brien, Jr, PhD

Objective. To evaluate the frequency dependence of ultrasonic backscatter for its ability to differentiate between neoplastic and healthy tissue. ***Methods.*** Standard B-mode images were created of 5 rats with spontaneous mammary tumors, and regions of interest in the lesion and surrounding tissue were parameterized by the slope of the backscatter amplitude versus frequency. ***Results.*** In 4 of the 5 rats, the averaged backscatter slope of the regions of interest in the tumor was significantly ($P < .05$) different from that of the surrounding tissue, and the fifth case had a moderate difference ($P = .20$). The consistency of the averaged slope values (1.2–1.8 dB/MHz) across all but 1 of the mammary tumors was encouraging for the prospect of identifying a tissue type by its backscatter slope. ***Conclusions.*** This work suggests that characterization and diagnosis of tissue types may be possible by using ultrasonographic images quantified by the frequency dependence of backscatter. ***Key words:*** quantitative imaging; rat mammary tumor; frequency-dependent backscatter.

Abbreviations
ROI, region of interest

Received October 12, 2000, from the Bioacoustics Research Laboratory, Department of Electrical and Computer Engineering (K.A.T., W.D.O.), and Department of Veterinary Pathobiology (J.F.Z.), University of Illinois at Urbana-Champaign, Urbana, Illinois. Revision requested November 20, 2000. Revised manuscript accepted for publication January 25, 2001.

We thank Kandice Norrell for assistance and advice with the animals and Jim Blue for the photographs and animal assistance. This work was supported in part by grants CA09067 and CA79179 from the National Institutes of Health.

Address correspondence and reprint requests to William D. O'Brien, Jr, PhD, Bioacoustics Research Laboratory, Department of Electrical and Computer Engineering, University of Illinois at Urbana-Champaign, 405 N Mathews Ave, Urbana, IL 61801.

Clinical ultrasonic scanners provide information, in principle, about the backscattered ultrasonic amplitude as a function of frequency. In most conventional applications, however, only the frequency-integrated or peak amplitude echogenicity is used to create an image. Cancer diagnoses, for example, rely on simple frequency-independent echogenicity of scanned features to decide whether a lesion is present and to determine its size. Any further assessment typically requires a biopsy.

In this study, we explored the possibility of extracting more information from the ultrasonographic image, namely by evaluating the frequency dependence of the backscattered ultrasound and using it to quantify the conventional B-mode image. The frequency dependence of backscatter may be used to characterize tissue (for example, see Insana et al[1] and Nassiri and Hill[2,3]), and such quantification of the tissue condition may ultimately provide a noninvasive aid in diagnosis.

The basic physics of scattering theory dictates that ultrasound waves will scatter in a manner dependent on their wavelength compared to the size of objects in their path. Several studies have evaluated the amplitude of the absolute backscatter coefficient in biological tissue to quantify properties such as tissue anisotropy[4–6] or to differentiate normal from diseased tissue,[7–9] but, to our knowledge, relatively few have used the frequency dependence of backscatter to extract information about tissue characteristics. Studies of tissue-mimicking phantoms,[10,11] the kidney,[1,12] and the eye[13] have investigated the relationship between backscatter spectra and tissue microstructure. In particular, these studies established that the slope of the backscatter amplitude with respect to the ultrasonic frequency can provide information about the effective scatterer size (also see Topp and O'Brien[4]).

One of the most interesting uses of quantitative ultrasonographic imaging was that of Feleppa and co-workers[14,15] in their large study of prostate tissue. They combined spectrum analysis (including frequency dependence) with a nonlinear classification scheme (based on the spectrum analyses and various medical variables such as specific antigen concentration) to distinguish between cancerous and noncancerous prostate tissue. Using very large tables computed by neural network scoring, they created likelihood-of-cancer scores, which were expressed in pixel values on images that depicted the probability of malignancy in the ultrasonographically imaged prostate.

Our technique is a much simpler version of quantitative imaging. In this pilot study of 5 rats, we explored the possibility of quantifying ultrasonographic images with selected regions of interest (ROIs) labeled only by their backscatter slope. The potential diagnostic value of such "parametric imaging" for various ultrasonic parameters has been shown previously in tissue-mimicking phantoms,[10] liver,[16] and in vitro human aortas.[7] To the best of our knowledge, images using the frequency dependence of backscatter to differentiate between regions with different scattering properties have been applied so far only to test phantoms,[10] prehyperthermia- and posthyperthermia-treated areas of in vitro liver, and a single ocular melanoma.[13] The goal of this work was to test the feasibility of differentiating in vivo between adjacent diseased (neoplastic) and healthy tissue in rats with spontaneous mammary tumors by creating such quantified images.

Materials and Methods

Animal Procedures

Rat mammary tumors were studied in vivo for this investigation. Five retired breeder female rats (Sprague Dawley; Harlan, Indianapolis, IN), in which spontaneous mammary tumors had developed, were acquired on notification from Harlan that such rats were available. The sizes and locations of the tumors were variable.

Each rat was anesthetized for the experiment with ketamine hydrochloride at 87 mg/kg and xylazine at 13 mg/kg. Hair from the skin covering the tumor and surrounding area was removed with electric clippers and a depilatory agent (Nair; Carter-Wallace, Inc, New York, NY). The anesthetized rat was then held upright and immersed in 37°C degassed distilled water such that its tumor faced the transducer (Fig. 1). The ultrasonic acquisition scan (see next section) lasted typically 30 minutes, after which the rat was killed under anesthesia by cervical dislocation, and its tumor was removed and fixed in 10%

Figure 1. Anesthetized rat 3 in holder, submerged to mid-abdomen in 37°C degassed distilled water. The head of the rat is above the region of the photograph, but the tail (T) is clearly visible near the bottom. The tumor in this case is very low on the left abdomen (outlined by white arrows). The 7.5-MHz transducer is shown at the bottom left (black arrow), focused within the tumor mass.

Table 1. Location of Tumors on Each Rat, Gross Appearance of Tumor Mass, and Histologic Notes

Rat	Tumor Location	Gross Appearance	Histologic Notes
1	Right midabdomen	Large, smooth	Lobular pattern prominent
2	Left axial	Small, softest	Fibrous connective tissue more prominent
3	Very low, left abdomen	Large, smooth	Lobular pattern more prominent
4	Lower left abdomen	Very large, irregular, ulcerated	Lobular pattern less prominent because of large areas of tissue necrosis, inflammation, and open tissue spaces
5	Right axial	Large, smooth	Lobular pattern more prominent

neutral buffered formalin for histologic evaluation. Table 1 indicates the location of the tumor on each animal, its gross appearance (including relative size), and notes from microscopic evaluation. Only tumors 4 and 5 were weighed after being excised, at 18 and 11 g, respectively. All rats (with tumors) weighed between 300 and 320 g, except rat 3, which weighed 380 g.

The experimental protocol was approved by the campus Laboratory Animal Care Advisory Committee and satisfied all campus and National Institutes of Health rules for the humane use of laboratory animals.

Acquisition of Data

A 7.5-MHz single-element wide-band transducer (V3322; Panametrics, Waltham, MA; 1.9-cm diameter, 5.1-cm radius of curvature) and a Panametrics 5900 pulser/receiver were used for all measurements. The anesthetized rat and the transducer were both immersed in a degassed distilled water bath, which was temperature controlled to 37 ± 0.5°C; the rat was held in a holder by its 4 paws with its teeth hooked over a wire loop, and the transducer was held in a micropositioning system that was translated laterally to the direction of the ultrasound beam (Fig. 1). The focus of the transducer was arranged to be approximately 5 to 10 mm below the proximal surface of the tumor so that, within the variable contours of the tumor and torso surface, the 10-mm –6-dB focal depth of the transducer interrogated the region 1 cm or so below the skin. The echo signals from the transducer were displayed on a digitizing oscilloscope (9354 TM; LeCroy, Chestnut Ridge, NY) set to sample at 100 megasamples/s. A dedicated personal computer (Dell, Round Rock, TX) recorded and stored the echo signals from the oscilloscope for processing off-line.

A lateral series of echo waveforms was recorded over both the tumor and some surrounding tissue in a standard B-mode configuration. Spacing between each recorded echo was chosen to be a half-wavelength (100 μm). The lateral distance covered and the recorded axial depth of the echo signal were chosen according to the particular morphology of the tumor of each rat.

When the animal experiment was completed, a series of reference reflections was recorded from a Plexiglas plate, positioned in 1-wavelength increments along the transducer axial direction. These reference echoes were taken starting from the position corresponding to the proximal surface of the B-mode image to the distal recorded echo of the image to calculate the absolute backscatter coefficient (and its slope versus frequency) of selected ROIs of the image using the method described in the next section.

Analysis of Data

The goal of the analysis was to produce a standard B-mode image with superimposed areas of selected ROIs marked by the value of their backscatter slope. To check the size of ROIs necessary to give ROI size–independent backscatter slopes, a homogeneous tissue-mimicking phantom[17] was used. A B-mode image was acquired, and concentric ROI squares ranging in size from 0.4 to 4.0 mm per side were analyzed for their respective slopes. For the 7.5-MHz transducer, it was found that 2 × 2-mm ROI boxes were sufficient (Fig. 2), which corresponded to 20 echo waveform sections (when lateral step size was 100 mm) of a time gate of 2.6 microseconds (260 sample points, 100 megasamples/s). Note that 2 mm is about 10 wavelengths in tissue for the 7.5-MHz transducer. A 10-wavelength distance was also found to give size-independent slopes in the

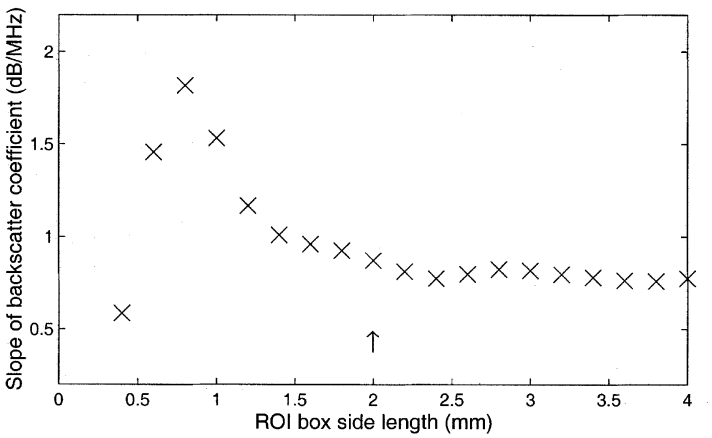

Figure 2. Calculated slope of the backscatter coefficient in a homogeneous tissue-mimicking phantom[17] by using concentric square ROIs of the indicated box side length. The arrow indicates the 10-wavelength distance for this ultrasonic frequency, which was chosen to be the square box side length for ROIs in this study.

homogeneous phantom for a 3.5-MHz transducer (4.3-mm ROI size) and a 10-MHz transducer (1.5-mm ROI size).

To reduce data storage and processing time, the B-mode images displayed for ROI selection were created by using a sliding Hanning window (with 50% overlap) along each echo signal to create larger image pixels than would be displayed on a standard B-mode image. The size of the sliding window was chosen to create approximately square pixels, as determined by the lateral distance between recorded waveforms (resulting in pixels 100 μm per side in this study). Each pixel was then the integrated Hilbert transform of the windowed sample points and was represented in decibels to form the image. The resulting image was practically indistinguishable from a B-mode image using all recorded samples.

The selected ROIs used all recorded sample points (by locating the echo waveform data from the original acquisition file that corresponded to the ROI area). The backscatter coefficient as a function of frequency over the ROI area was calculated according to the method of Insana and Hall[10,11]:

$$\sigma_b(f) = \frac{0.36 R_1^2 \gamma^2}{A_o \Delta z} e^{+4(\alpha_m - \alpha_o)(R_s + \Delta z/2)} \frac{\left\langle |S(f)|^2 \right\rangle}{|R(f)|^2},$$

where R_1 was the distance between the transducer and the near surface of the ROI; A_o was the area of the transducer aperture; Δz was the axial length of the ROI; R_s was the distance from the front water-tissue interface to the near surface of the ROI; α_m and α_o were the frequency-dependent attenuation coefficients of the tissue (assumed to be 0.7 dB · cm^{-1} · MHz^{-1} in all cases) and water, respectively; and $\langle |S(f)|^2 \rangle$ was the averaged power spectral estimate from the laterally sampled, Hanning-gated, backscattered waveforms within the ROI. $|R(f)|^2$ was the reference power spectral estimate obtained from the reflection against the Plexiglas plane reflector, with an amplitude reflection coefficient of $\gamma = 0.35$, evaluated at axial distance $R_1 + \Delta z/2$. See Figure 3 for an example of $|R(f)|^2$ and $\langle |S(f)|^2 \rangle$ from a rat mammary tumor.

Regions of interest were selected on the image by choosing areas that were approximately homogeneous over the 2 × 2-mm ROI and within approximately 10 mm of the proximal skin surface. For each ROI, the backscatter coefficient was calculated, and its slope versus frequency was used to label the ROI box on the image. Figure 4 shows an example of the backscatter coefficient in a tumor versus frequency (using the power spectra shown in Fig. 3) and the best-fit (least squares) slope.

After each image was produced and labeled with ROIs, the mean and SEM of the slope parameters were calculated for ROIs inside and outside the tumor. A statistical comparison between the ROI slopes in the neoplastic and normal regions for each rat was performed by using a Student *t* test analysis (2-sample, unequal variance).

Results

A B-mode image of each rat tumor and surrounding tissue was produced and labeled with ROIs in regions both inside and outside the tumor. The image of rat tumor 1 is shown for example in Figure 5. In rats 1, 3, 4, and 5, the tumors are obvious in the images by their hypoechogenicity compared with that of the surrounding tissues. The tumor in rat 2, however, has considerably higher echogenicity and is much more heterogeneous in its B-mode image than the others.

To assess whether there was a significant difference in the backscatter slopes of the ROIs within the tumors versus the surrounding tissue, the ROI slopes in each region were averaged and

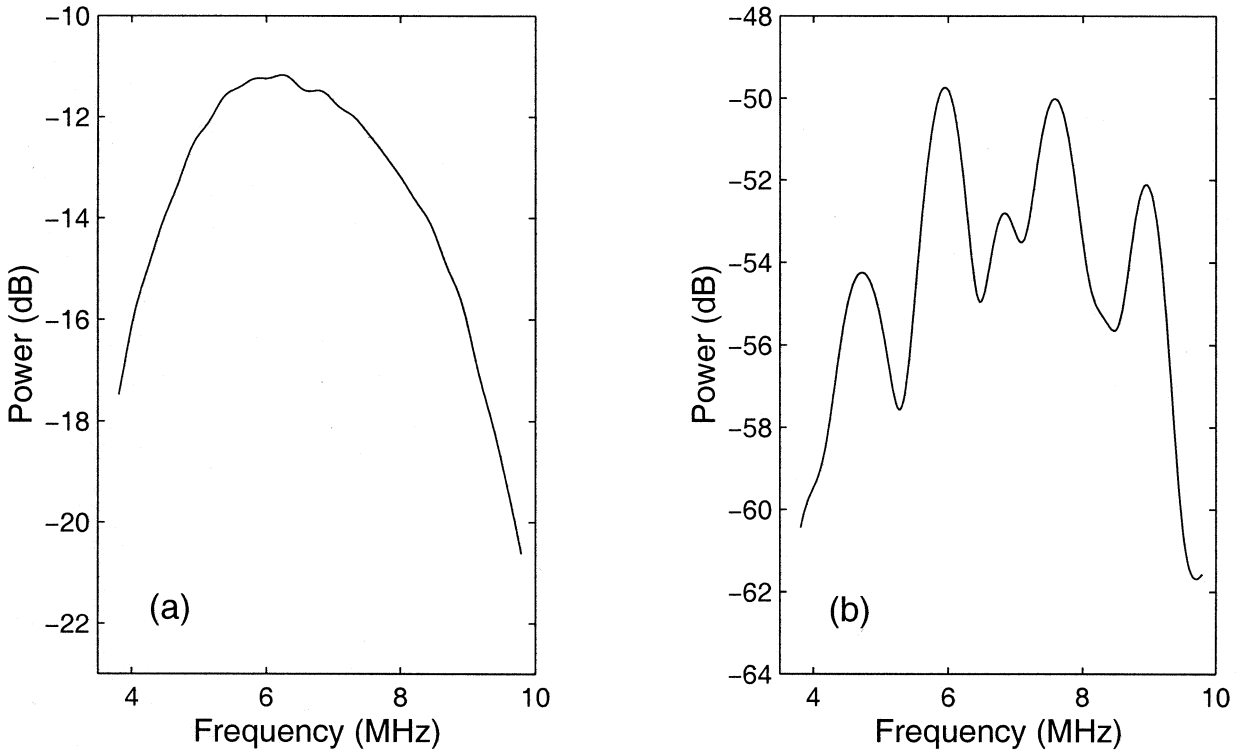

Figure 3. Examples of the power spectrum of the 7.5-MHz transducer reflecting from the Plexiglas plate (**A**) and the power spectrum of an ROI in rat tumor 4 at the same axial location (**B**). The spectrum from the tissue is an average of 20 Hanning-gated echo signals within the 2 × 2-mm ROI.

compared (Fig. 6). The number of ROIs in the region outside the tumor, which is typically normal mammary gland and subcutaneous adipose tissue, was usually limited by the heterogeneity of anatomic structures, such as bone-tissue interfaces, or the anechogenicity of the bladder. It is evident that the averaged backscatter slopes over the tumor regions for rats 1, 3, 4, and 5 were quite similar, between 1.2 and 1.8 dB/MHz. Rat 2, whose tumor was seen under histologic evaluation to have much more connective tissue (collagen) than the others, had an obviously lower slope value. The regions outside the tumors were notably different from each other (ranging from –0.44 to 1.7 dB/MHz), but this should not be surprising, because in this initial study, the spontaneous tumors were in different locations on the rats. In all the rats, except perhaps rat 5 ($P = .20$), there was a significant difference in the averaged ROI slopes from regions inside the tumor versus outside ($P < .05$).

Histologic sections were made of each tumor in the plane of the ultrasonographic image. Figure 7 shows tumor 1 under 2 magnifications:

Figure 4. Example of the calculated backscatter coefficient (equation in "Materials and Methods") of an ROI as a function of frequency from rat tumor 4. (The relevant power spectra are those shown in Fig. 3.) The least squares slope is indicated by the dotted line. The value of the slope is used to parameterize the selected ROI.

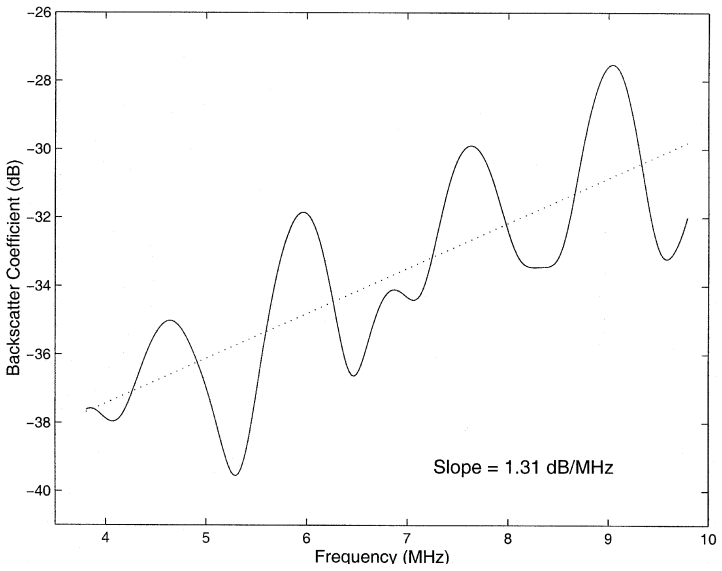

the larger field of view (Fig. 7A) shows the tumor to be well demarcated from the overlying skin and partially encapsulated with connective tissue. The skin above the tumor consists of the epidermis, dermis with subcutaneous adipose tissue containing hair follicles, and subcutaneous muscle (the latter is the thin, even layer, approximately 0.25 mm thick). The tumor is formed of discrete coalescing lobules of various sizes that contain neoplastic mammary epithelial cells. Figure 7B is a higher magnification of the same tumor within 1 lobule. Neoplastic mammary epithelial cells are seen arranged in small clusters and ductules, which are separated by vascularized connective tissue. Each tumor was found on histologic examination to have this same general structure: a fibrous tissue encapsulated mass divided into lobules by connective septa, each lobule further subdivided into smaller lobules by connective tissue septa, and each smaller lobule containing groups of mammary epithelial cells. The differences in each case are noted in Table 1.

Discussion

We have studied the frequency dependence of ultrasonic backscatter from a standard B-mode acquisition to evaluate the feasibility of characterizing tissue from the slope of the backscatter amplitude versus frequency. Five rats with spontaneous mammary tumors were used in this study.

In at least 4 cases, the averaged slope of ROIs in the tumor was statistically significantly different from that of the surrounding tissue. This result is promising for the ability to differentiate between tissue types or morphologies on the basis of the parameter of backscatter slope. The scatter of the slope values, however, within areas that appeared to be homogeneous (for example, the dark tumor mass in Fig. 5), was broader than we had hoped. Ideally, we would want each ROI to give significant and reliable information.

Figure 5. A, B-mode image of rat 1. The image was formed by scanning the transducer horizontally (lateral-medial plane) from outside the right of the torso, over the mass, to the midline of the abdomen. The top and left dark portions are the surrounding water; the dark area with closely packed ROIs is the tumor; and the brighter region on the right is the midabdominal area. The right bar indicates the relative reflection magnitude of each image pixel in decibels. **B**, Same image as above, with selected ROIs labeled by the value of the backscatter slope.

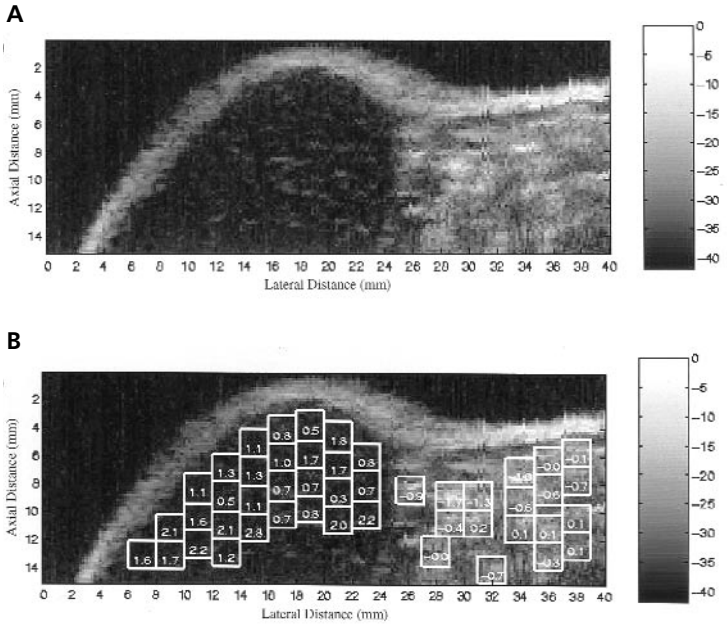

Figure 6. Values of the backscatter slope averaged over ROIs selected from inside (dark bars) and outside (light bars) the tumor region. Error bars represent the SEM over the ensemble within each region. The number of ROIs in each case varied from 29 to 41 inside the tumor to 9 to 18 outside the tumor.

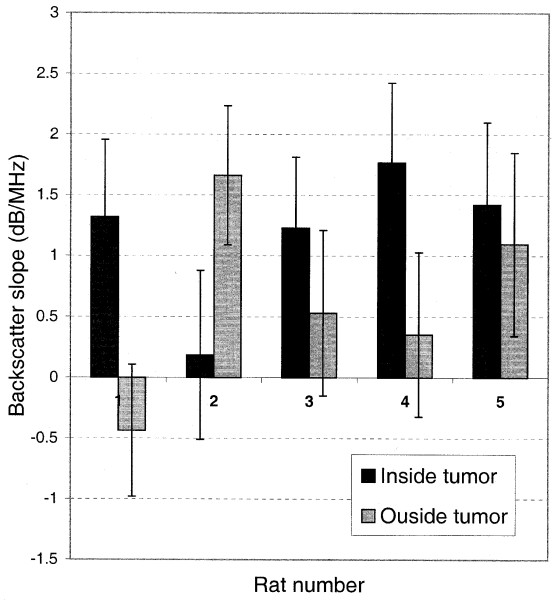

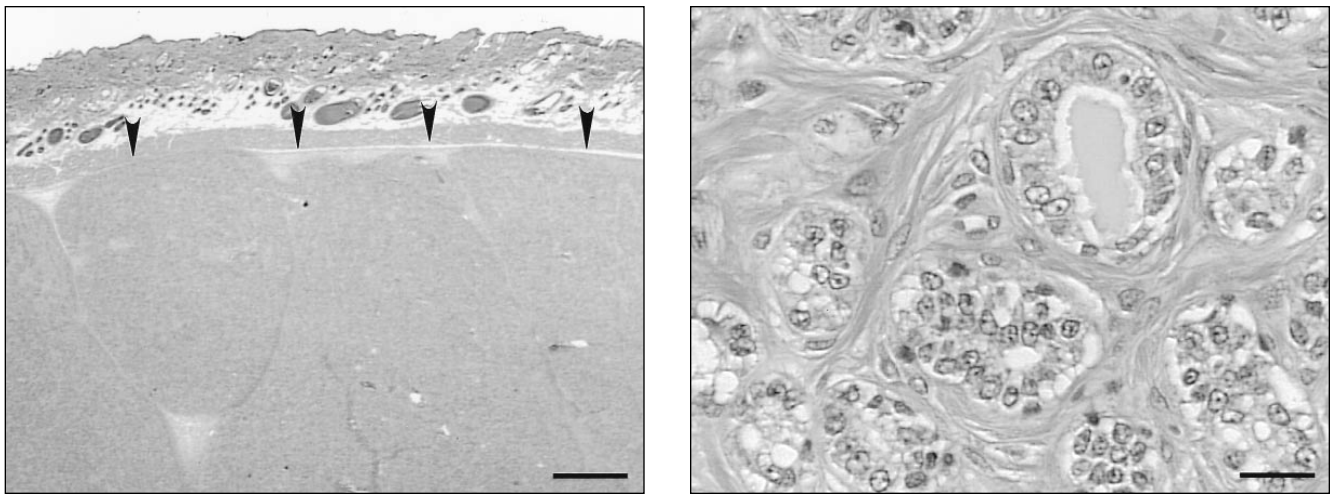

A **B**

Figure 7. Photomicrographs of rat mammary tumor 1. **A**, Tumor and overlying skin. Scale bar indicates 4 mm. Arrows delineate the tumor border. **B**, Higher magnification of the same tumor. Scale bar indicates 100 μm. The specimen was fixed in 10% neutral buffered formalin, dehydrated, embedded in paraffin, sectioned at 3 mm in the plane of the B-mode ultrasonographic acquisition, mounted on glass slides, and stained with hematoxylin-eosin for microscopic evaluation.

Even though the test of ROI sizes in a homogeneous tissue-mimicking phantom indicates that the slope becomes size independent, for the 7.5-MHz transducer at 2 mm, the spectra from tissue are inherently noisy. We found in the homogeneous tissue-mimicking phantom[17] that the backscatter slope was more robust for spectra averaged over widely spaced (i.e., larger than the transducer spot size), laterally sampled radio frequency echoes. In disease diagnosis, however, we are limited to the size of the lesion in the tissue for the amount of possible spatial averaging. This brings up a fundamental difficulty of wanting large spatial sampling volumes as opposed to very localized tissue characterizations. Our findings suggest the following compromise: use the smallest ROI sizes that appear to give a size-independent slope; mark homogeneous areas of the target tissue region with slope-labeled ROIs; and use simple statistical averaging of ROI slopes to find a resulting slope parameter that describes the larger tissue region of interest.

The consistency of average slope values (1.2–1.8 dB/MHz) across all but 1 of the rat mammary tumors is encouraging for the prospect of identifying a tissue type by its backscatter slope. Outlying rat tumor 2 was found on histologic examination to have much more connective tissue infiltrating the tumor than the others. Because marked interfaces between tissue types give stronger reflected signals with, in principle, a flatter backscatter frequency response,[18] the abundance of connective tissue may explain the lower slope values for rat tumor 2. The higher slope in the normal tissues of rat 2 is not understood but may be related to the fact that the location of the tumor in rat 2 was the most anterior of the 5 tumors studied, and it appeared to be surrounded by more fat tissue than the others.

Directions for future studies should include a more careful evaluation of the attenuation of regions overlying each ROI. Backscatter spectra were compensated for energy loss in tissue between the transducer and selected ROI by using a standard soft tissue attenuation coefficient of 0.7 $dB \cdot cm^{-1} \cdot MHz^{-1}$. (Values tested here between 0.4 and 1.0 $dB \cdot cm^{-1} \cdot MHz^{-1}$ decreased or increased the slopes of all ROIs within 10 mm of the surface by only a few percent and did not noticeably affect the difference in slopes between healthy and cancerous regions, which is the basis for our method.) A more specific evaluation of the overlying regions (by the multi–narrow-band method,[7] for example) may produce more robust slope values.

This pilot study showed a statistical difference in backscatter slope values between regions within rat mammary tumors and in the surrounding tissue. Because the spontaneous tumors occurred in different locations in each rat, however, we could not make a meaningful

analysis of the slope parameters in the surrounding healthy tissues. Future work will study tumors grown in a controlled manner on the same tissue (say, the liver) within each rat. This type of managed study should give a better comparison of the slope parameter in healthy versus diseased tissue.

The current work suggests that it may be possible to discern a difference in the frequency dependence of backscattered sound between cancerous tissue and its surroundings. The use of this parameter for quantitative imaging may aid in the identification of various tissues and their conditions and, it is hoped, could eventually be used for noninvasive diagnoses of disease.

References

1. Insana MF, Hall TJ, Fishback JL. Identifying acoustic scattering sources in normal renal parenchyma from the anisotropy in acoustic properties. Ultrasound Med Biol 1991; 17:613–626.
2. Nassiri DK, Hill CR. The differential and total bulk acoustic scattering cross sections of some human and animal tissues. J Acoust Soc Am 1986; 79: 2034–2047.
3. Nassiri DK, Hill CR. The use of angular acoustic scattering measurements to estimate structural parameters of human and animal tissues. J Acoust Soc Am 1986; 79:2048–2054.
4. Topp KA, O'Brien WD Jr. Anisotropy of ultrasonic propagation and scattering properties in fresh rat skeletal muscle in vitro. J Acoust Soc Am 2000; 107: 1027–1033.
5. Mottley JG, Miller JG. Anisotropy of the ultrasonic backscatter of myocardial tissue: I. Theory and measurements in vitro. J Acoust Soc Am 1988; 83: 755–761.
6. Madaras EI, Perez J, Sobel BE, et al. Anisotropy of the ultrasonic backscatter of myocardial tissue: II. Measurements in vivo. J Acoust Soc Am 1988; 83: 762–769.
7. Bridal SL, Fornès P, Bruneval P, Berger G. Parametric (integrated backscatter and attenuation) images constructed using backscattered radio frequency signals (25–56 MHz) from human aortae in vitro. Ultrasound Med Biol 1997; 23:215–229.
8. Lu ZF, Zagzebski JA, Lee FT. Ultrasound backscatter and attenuation in human liver with diffuse disease. Ultrasound Med Biol 1999; 25:1047–1054.
9. D'Astous FT, Foster FS. Frequency dependence of ultrasound attenuation and backscatter in breast tissue. Ultrasound Med Biol 1986; 12:795–808.
10. Insana MF, Hall TJ. Parametric ultrasound imaging from backscatter coefficient measurements: image formation and interpretation. Ultrason Imaging 1990; 12:245 - 267.
11. Insana MF, Wagner RF, Brown DG, Hall TJ. Describing small-scale structure in random media using pulse-echo ultrasound. J Acoust Soc Am 1990; 87: 179–192.
12. Hall TJ, Insana MF, Harrison LA, Cox GG. Ultrasonic measurement of glomerular diameters in normal adult humans. Ultrasound Med Biol 1996; 22: 987–997.
13. Lizzi FL, Astor M, Liu T, et al. Ultrasonic spectrum analysis for tissue assays and therapy evaluation. J Imaging Syst Technol 1997; 8:3–10.
14. Feleppa EJ, Fair WR, Tsai H, et al. Progress in two-dimensional and three-dimensional ultrasonic tissue-type imaging of the prostate based on spectrum analysis and nonlinear classifiers. Mol Urol 1999; 3: 303–310.
15. Feleppa EF, Fair WR, Liu T, et al. Two-dimensional and three-dimensional tissue-type imaging of the prostate based on ultrasound spectrum analysis and neural-network classification. In: Shung KK, Insana M (eds). Medical Imaging 2000: Ultrasonic Imaging and Signal Processing. Vol 3982. Bellingham, WA: Society of Photo-Optical Instrumentation Engineers; 2000:152–160.
16. Lizzi FL, King DL, Rorke MC, et al. Comparison of theoretical scattering results and ultrasonic data from clinical liver examinations. Ultrasound Med Biol 1988; 14:377–385.
17. Madsen EL, Dong F, Frank GR, et al. Interlaboratory comparison of ultrasonic backscatter, attenuation, and speed measurements. J Ultrasound Med 1999; 18:615–631.
18. Lizzi FL, Astor M, Kalisz A, et al. Ultrasonic spectrum analysis for assays of different scatterer morphologies: theory and very-high frequency clinical results. In: 1996 IEEE Ultrasonics Symposium Proceedings. Piscataway, NJ: Institute of Electrical and Electronics Engineers; 1996:1155–1159.